Standard thermodynamic quantities as determined via models of nuclear multifragmentation

J. B. Elliott[1] and A. S. Hirsch[2]

[1]*Nuclear Science Division, Lawrence Berkeley National Laboratory, Berkeley, California 94720*
[2]*Purdue University, West Lafayette, Indiana 47907*
(Received 30 November 1999; published 5 April 2000)

Both simple and sophisticated models are frequently used in an attempt to understand how real nuclei breakup when subjected to large excitation energies, a process known as nuclear multifragmentation. Many of these models assume equilibrium thermodynamics and produce results often interpreted as evidence of a phase transition. This work examines one class of models and employs standard thermodynamical procedures to explore the possible existence and nature of a phase transition. The role of various terms, e.g., Coulomb and surface energy, is discussed.

PACS number(s): 25.70.Pq, 64.60.Ak, 24.60.Ky, 05.70.Jk

I. INTRODUCTION AND OVERVIEW

Many models [1–9] have been proposed to describe the breakup of a large nucleus subjected to excitation energies greater than a few MeV per nucleon, a process known as multifragmentation. Experimentally, the signature of multifragmentation is the production of a wide range of nuclear reaction products, particularly intermediate mass fragments (IMFs), $3 \leq Z \leq 30$. On the basis of inclusive data, it was proposed [10–12] that these fragments were produced in analogy to a liquid-to-gas phase transition occurring in a nucleus. A recent experiment that permitted the total charge reconstruction of each event studied multifragmentation resulting from the breakup of gold nuclei as a function of the excitation energy deposited [13–17]. The statistical aspects of these data have provided strong evidence that multifragmentation is indeed related to a phase transition occurring in a finite system. Whether the production of IMFs in such collisions is due to a phase transition, and if so, what type, is still an issue of much debate [18].

One class of models developed to explore the fate of a nucleus as a function of excitation energy is based on the phenomenological description of the free energy $F(V,T)$ of the breakup state, where T is the common temperature of all nucleons and nuclei within the breakup volume V. These nuclei are considered to be at normal nuclear density and interact only via the Coulomb force. The distribution of nuclear fragments prior to any secondary decay can then be calculated as a first step in the disassembly of the excited initial system. To compare with data, deexcitation of fragments and expansion of the system due to the Coulomb repulsion between the fragments must be accounted for in the model. However, if the thermodynamics of the model is of interest, as is the case in this work, then only the behavior of thermodynamic variables need be examined, e.g., free energy, entropy, specific heat, pressure, isothermal compressibility. Thus, no fragment distributions need be explicitly calculated and therefore no fragment distributions are analyzed in this work.

Here, several variations of a previously discussed model [8] are explored. A canonical ensemble approach is used to investigate the thermodynamics of the system where the free energy, F, is written as a function of the temperature, T, and the volume, V. Calculations are restricted to a system which contains 162 constituents, since this is representative of the size of the system studied in Ref. [16]. Contributions to F, e.g., the surface free energy, the Coulomb energy, are examined by turning them off or altering the form of the contribution in question. In this way insight can be gained as to how the important features of the thermodynamics such as specific heat, isothermal compressibility, etc., depend on the parametrization of the free energy.

This paper is organized as follows. In Sec. II the details of the models are presented. Three versions of a standard statistical multifragmentation model are examined as well as a well-known mean field model whose results are used for comparison. In Sec. III a description of the analysis and the results of that analysis are presented. Section IV discusses the standard interpretations of the models and analysis. Finally, a brief discussion of the questions raised by this work concludes this paper. In general, the notation of Refs. [1] and [8] are followed.

II. DETAILS OF THE MODELS

This work follows directly the efforts presented in Ref. [8] in which the canonical partition function was examined as a function of temperature in a fixed volume system for evidence of a phase transition. In that work, evidence for a first order phase transition was found. In the present work, the volume (average density) of the system is permitted to vary. It shall be seen that the nature of the phase transition depends on the volume of the system. The work of Ref. [8] is also extended by examining the effects of the Coulomb force on the system and the effects of the choice of surface energy parametrizations. The units used for the nuclear models are: energy and free energy in MeV/nucleon, temperature in MeV, volume in fm^3, pressure in MeV/fm^3, and so on. A general description of each system follows.

A. V1: Full statistical description of an excited nucleus

Calculations begin by considering the free energy of a nuclear fragment. It is assumed [1] that the free energy of a nuclear fragment of mass A and charge Z, for $A > 1$ is given by

$$F_{A,Z} = F_{A,Z}^B + F_{A,Z}^{sym} + F_{A,Z}^S + E_{A,Z}^C. \qquad (1)$$

The terms in Eq. (1) refer to the bulk, symmetry, surface, and Coulomb contributions to the free energy of a nuclear fragment. The forms of these terms are [1]

$$F_{A,Z}^B = (-W_0 - T^2/\epsilon_0)A, \qquad (2)$$

$$F_{A,Z}^{sym} = \gamma(A - 2Z)^2/A, \qquad (3)$$

$$F_{A,Z}^S = \beta_0 \left(\frac{T_c^2 - T^2}{T_c^2 + T^2} \right)^{5/4} A^{2/3}, \qquad (4)$$

$$E_{A,Z}^C = \frac{3}{5} e^2 Z^2 (1 - (1 + \kappa)^{-1/3}) / R_{A,Z}. \qquad (5)$$

In Eq. (2) the constants are taken as $W_0 = 16$ MeV and $\epsilon_0 = 16$ MeV. In Eq. (3) $\gamma = 25$ MeV. In Eq. (4) $\beta_0 = 18$ MeV and $T_c = 16$ MeV, following Ref. [9]. The contribution from the Coulomb term is estimated via a Wigner-Seitz approximation as in Ref. [1].

The κ term is related to the volume of the system through

$$1 + \kappa = V/V_0. \qquad (6)$$

The simplified model presented here differs from the standard version [1] in that there is only one parameter relating the volume excluded by the constituents V_0 to the total volume of the system V and to the free volume V_f. Here the free volume is the difference between the total volume V and the sum of the volume of the fragments, assumed to be at normal nuclear density, and is the volume available for the translational motion of the fragments.

In the standard version of the model the free volume is given by $V_f = \chi V_0$, where χ is parametrized to increase with fragment multiplicity such that it varies between 0.2 and 2; the parameter κ is fixed, usually at $\kappa = 2$. For simplicity, here it is assumed that $\kappa = \chi$ so that specifying V_f determines the value of κ in Eq. (6). See Ref. [1] for details of κ and χ in the standard version.

For this work then, the total volume of the system is given by

$$V = V_0 + V_f. \qquad (7)$$

Two things become obvious from Eq. (7); first, with this form of V the free energy of the system varies with V_f since V_0 is a constant. Second, the loss of free volume in the closest packing of spherical clusters is ignored. The issue of whether spherical nuclei can actually be placed in a total volume V_0 given a free volume V_f is not addressed. Undoubtedly, there will be situations where it is not possible for the total volume to accommodate all of the nuclear clusters. The purpose here, however, is to explore the thermodynamics and self-consistency of the model and not physical consistency.

Finally $R_{A,Z}$ is the radius of the fragment in question and is determined by

$$R_{A,Z} = r_0 A^{1/3}, \qquad (8)$$

with $r_0 = 1.17$ fm. The version of the model presented above will be termed V1.

From this point the intrinsic partition function of a fragment of A, Z at temperature T, and volume V can be determined [8] as follows:

$$z_{A,Z} = \exp(-F_{A,Z}/T). \qquad (9)$$

Using a technique developed in Ref. [19] and used on a simplified version of this model [8], the canonical partition function can be built via a recursion relation

$$\mathcal{Z}_p = \frac{1}{p} \sum_{A=1}^{p} A \omega_A \mathcal{Z}_{p-A}, \qquad (10)$$

starting from $\mathcal{Z}_0 = 1$. Here for calculational simplicity the approximation has been made that for each and every fragment with $A > 1$, $A/Z = 2.5$ which represents an average mass to charge ratio for fragments. The ω_A term is

$$\omega_A = \frac{V_f}{h^3} (2\pi m T)^{3/2} A^{3/2} z_{A,Z}, \qquad (11)$$

where the terms on the left of the fragment partition function, $z_{A,Z}$, account for the translational free energy contribution F^{tr}. It is now straightforward to calculate the partition function of the system for a given T, V_f, A_0, and Z_0. The free energy of the system of p particles is then determined as usual

$$F = -T \ln(\mathcal{Z}_p) + E_0^c(V), \qquad (12)$$

where the last term is the usual Coulomb contribution of a uniformly charged sphere

$$E_0^C(V) = \frac{3}{5} \frac{Z_0^2 e^2}{R}, \qquad (13)$$

with $R = (3V/4\pi)^{1/3}$.

1. Comparison of V1 to the full version of the model

The model and calculations described above were compared to the full, or unmodified version of the model often cited in the literature, see for example Refs. [1, 20–22], In Fig. 1 results from the full version of this model are shown for the mean fragment distribution calculated at a given input excitation energy. To generate event-by-event distributions Poissonian fluctuations about the mean are introduced, after which, temperature is adjusted to ensure energy conservation. To more fully recover the standard version of the model most often used, higher order corrections were introduced just as in the full version of the model; e.g., ϵ_0 in Eq. (2) was made dependent on the fragment mass A, for light clusters, $A \leq 4$, the empirical masses and binding energies, radii and spin degeneracy factors of the ground state were used, the total volume was held constant at $3V_0$, and the free volume was set to depend on the input excitation energy. Finally,
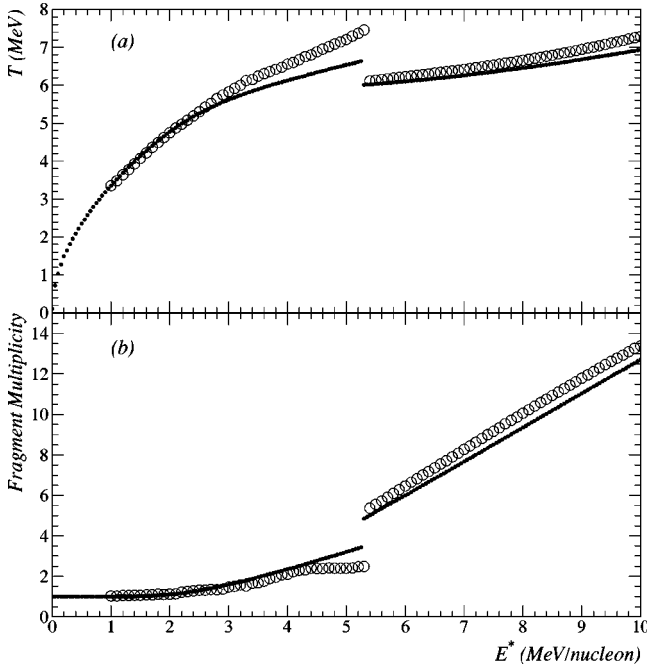
FIG. 1. Comparison of the full model (open circles) before Poissonian smearing and the calculations of this paper (full circles) for the caloric curve (a) and the average fragment multiplicities (b).
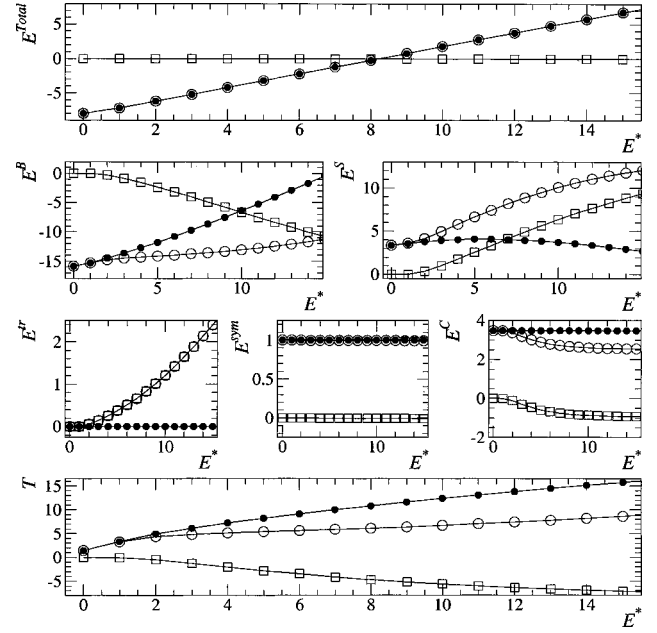

FIG. 2. Energy conservation in V1, overall, component by component (total, bulk, surface, translational, symmetry, and Coulomb energies, respectively) and the caloric curves. Full circles represent the initial state, open circles represent the final state and open squares represent the difference between the two.

energy was explicitly conserved; an input excitation energy was given and a temperature was determined such that total energy was conserved. The explicit conservation of energy produced results that were the same as those resulting from the unconstrained canonical ensemble.

Figure 1(a) shows the caloric curve from the full version of this model for a system with 100 nucleons (60 neutrons and 40 protons) compared to the same size system used in calculations with a modified version of V1. The general trend of the modified V1 reproduced the average behavior of the full model, though there is not a perfect agreement. This is to be expected. While this modified version of V1 is closer to the model, there are still some differences, e.g., the charge of $A > 4$ fragment is treated in only an average fashion in V1. The reproduction of the general trends indicates that V1 captures the essence of the full model. Figure 1(b) shows the fragment multiplicity, before any secondary decay, from both models. Again there is general agreement between the two.

The break observed in the caloric curve shown in Fig. 1 is well known in the full model, see, for example, Fig. 4 in Ref. [20] and Fig. 11 in Ref. [22]. The break is due to the initial guess of the system's multiplicity which is in turn used to guess the system's free volume. For low energies the multiplicity is chosen to be 1, 2, or 3 [Fig. 1(b) shows that the initial guess of the multiplicity is consistent with the final state multiplicity], while at higher energies the multiplicity depends smoothly on a function of the input excitation energy [1]. In some systems, e.g., a system of 100 nucleons, there is a jump in multiplicity at the transition from the low energy computations and the high energy computations which gives rise to a jump in the final state multiplicity, Fig. 1(b), and a break in the caloric curve, Fig. 1(a). When the

simplified model used in this work is given the same volume dependence as the full model, the results of the full model are reproduced.

Energy conservation is explored in Fig. 2. Here the unmodified version of V1 was used with a system of 162 particles and energy was explicitly conserved as outlined above. In order to examine the change in energy between the initial and final state of each term contributing to the system's total energy, the temperature of the initial state of the system has been calculated corresponding to the input E^*. The assumption that the initial nuclear state is in thermal equilibrium prior to its deexcitation to the final state has no bearing on the thermodynamics of the final state and is done only for purposes of the abovementioned calculation. The initial state used for this calculation was the system of 162 nucleons at excitation energy E^*, at normal nuclear density ρ_0, and at a temperature that conserves energy when the total energy is determined using Eqs. (2)–(5), (12), and

$$E = F - T \left(\frac{\partial F}{\partial T} \right)_V. \tag{14}$$

The total energy of the initial state is shown in Fig. 2 as well as its various components and a caloric curve. The final state of the system was computed with the same E^* but was held at a third normal density, $\rho_0/3$, and allowed to fragment in the manner outlined above. The caloric curve produced for the final state via this explicit conservation of energy calculation is identical to the caloric curve produced via the calculations without an explicit conservation of energy. Figure 2 shows that the temperature in the final state is lower than that in the initial state. Further inspection indicates that while

the Coulomb energy is reduced by creating smaller charged nuclei, the energy required to create the additional surface area more is more than offsetting. Thus, the temperature must decrease.

B. V2: Description of an excited charge-free nucleus

The general ideas of V1 are followed but with the Coulomb energy of the system set to zero. The free energy shown in Eq. (1) then becomes

$$F_A = F_A^B + F_A^S. \tag{15}$$

And the total free energy of the system is given by

$$F = -T \ln(\mathcal{Z}_p). \tag{16}$$

Every other aspect of the model is the same as in V1. This version of the model will be termed V2.

C. V3: Description of an excited charge-free nucleus with a temperature independent surface

In this version, the Coulomb force is suppressed and the temperature dependent surface term in Eq. (4) is made independent of temperature

$$F_A^S = \beta_0 A^{2/3}. \tag{17}$$

The free energy of a fragment and the entire system are still given by Eqs. (15) and (16). Every other aspect of the model is the same as in V1 and V2. This version of the model will be termed V3.

D. The van der Waals fluid

The free energy of the van der Waals fluid is determined in the standard textbook fashion. Starting from the free energy [23]

$$F/A = -t\{\ln[n_Q(V-Ab)/A]+1\} - Aa/V, \tag{18}$$

with $t = k_b T$, $n_Q = (Mt/2\pi\hbar^2)^{3/2}$, and a and b the usual van der Waals constants. In this work, Eq. (18) is computed in terms of the density, $\rho = A/V$, so that the number of constituents A is not a factor. For the van der Waals' constants a and b, values were used for helium so that $T_c \sim 4.5 \times 10^{-4}$ eV/nucleon. This also suggested the value of M in n_Q. Finally, Eq. (18) was evaluated in terms of T/T_c and V/V_c. The van der Waals fluid model is well defined and free of internal inconsistencies. It will be used as a benchmark for the analysis presented in this paper. Units for the van der Waals fluid results will be in eV/nucleon for energy and free energy, eV/nucleon$\times V_c$ for pressure, and so on.

III. DISCUSSION OF CALCULATIONS

Calculations were performed for each version of the model to determine $F(T, V_f, A_0, Z_0)$ for $A_0 = 162$, $A_0/Z_0 = 2.5$, and over a range in temperature, 1 MeV $\leq T \leq 14$ MeV, and volume of $2 \times 10^{-8} \leq (V_f/V_0) \leq 2 \times 10^8$. Once the
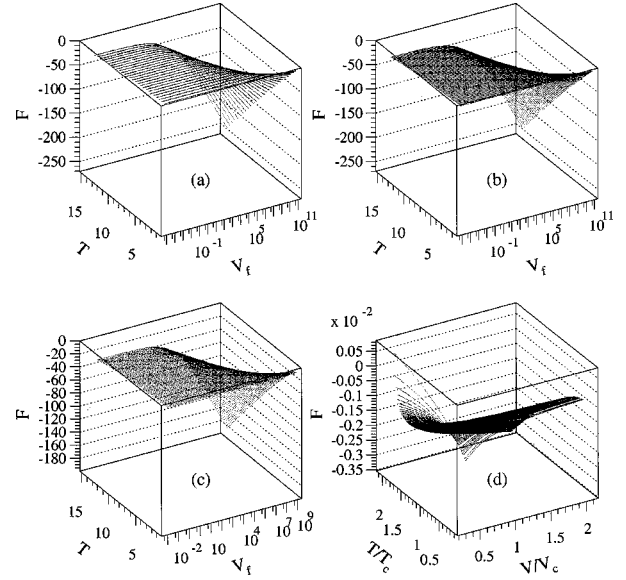

FIG. 3. Free energy surfaces as a function of temperature and volume for (a) V1, (b) V2, (c) V3, and (d) the van der Waals fluid.

general vicinity of the critical point was identified, a smaller range in (T, V_f) was used for more detailed calculations. For the van der Waals fluid the range was smaller and in terms of reduced temperature and volume: $0.1 \leq T/T_c \leq 2.0$ and $0.34 \leq V/V_c \leq 2.0$. Figure 3 shows the behavior of the free energy over the ranges of temperature and volume used in the calculations.

After the value of the free energy was calculated, it was simple to determine other thermodynamic quantities. Holding the volume fixed the entropy is given by the usual relation

$$S = -\left(\frac{\partial F}{\partial T}\right)_{V_f}. \tag{19}$$

In the case of this work differences were used instead of derivatives due to the numerical nature of the calculation, thus Eq. (19) becomes

$$S = -\left(\frac{\Delta F}{\Delta T}\right)_{V_f}. \tag{20}$$

Similarly the specific heat at constant volume was determined via

$$C_V = \langle T \rangle \left(\frac{\Delta S}{\Delta T}\right)_V, \tag{21}$$

where $\langle T \rangle$ is the average value of T over the ΔT interval. Using the entropy and the free energy, the total energy can be determined from
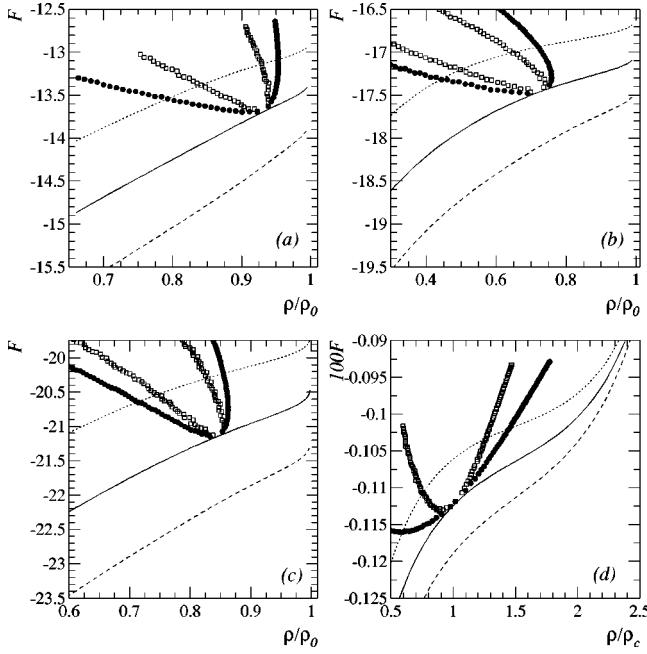
$$E = F + TS. \tag{22}$$

FIG. 4. Free energy isotherms as a function of reduced density for (a) V1, (b) V2, (c) V3, and (d) the van der Waals fluid. Open squares show the spinodal, full circles show the boundary of the coexistence region. Dotted curves are subcritical. Solid curves are critical. Dashed curves are supercritical.

In these calculations it was possible to hold either the temperature or the volume constant. The pressure was then found by holding the temperature fixed

$$P = -\left(\frac{\Delta F}{\Delta V_f}\right)_T. \qquad (23)$$

Taking another *derivative* then gave the isothermal compressibility

$$\kappa_T = -\frac{1}{\langle V_f \rangle}\left(\frac{\Delta V_f}{\Delta P}\right)_T, \qquad (24)$$

where $\langle V_f \rangle$ is the average value of V_f over the ΔV_f interval. With this information it is possible to determine if there is a phase transition in a model such as this and, if present, the nature of that phase transition. The following section addresses this question.

IV. RESULTS OF CALCULATIONS

In this section, each of the axes of the standard phase diagram T, V, and P, will in turn be held fixed. The behavior of other quantities will be examined in order to understand the behavior of each system. The van der Waals fluid will serve as a guide for the interpretation of the analysis and also as a benchmark to illustrate the accuracy of this analysis.
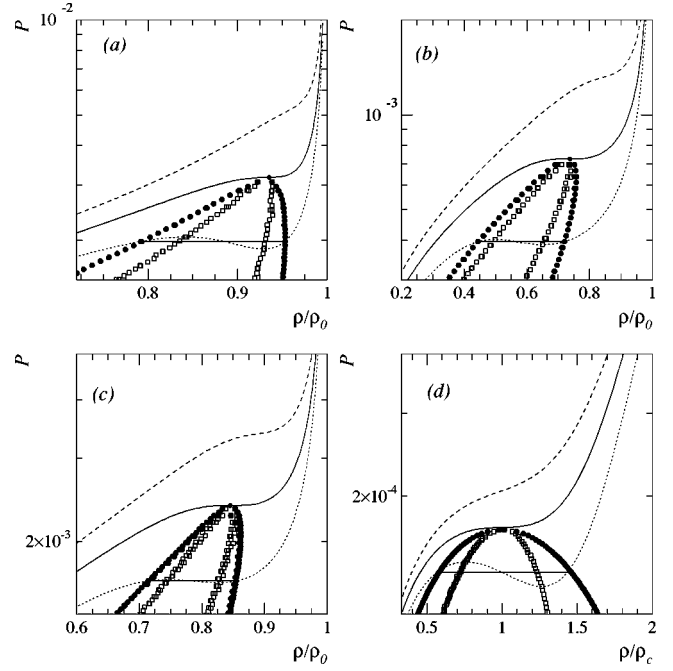

FIG. 5. Isotherms of pressure as a function of reduced density for (a) V1, (b) V2, (c) V3, and (d) the van der Waals fluid. Open squares show the spinodal, full circles show the coexistence curve. The solid horizontal line is an example of a Maxwell equal area construction to determine the coexistence region and find the critical point. Dotted curves are subcritical. Solid curves are critical. Dashed curves are supercritical.

A. Isotherms

Determination of the critical point, coexistence and spinodal curves is discussed below. The variation of the free energy as a function of density shows the same general features for these systems.

Figure 4 shows the behavior of the free energy isotherms for each system as a function of reduced density. Each plot in Fig. 4 shows three isotherms. The isotherms are subcritical ($T = 0.95T_c$), critical ($T = T_c$), and supercritical ($T = 1.05T_c$). Determination of the critical point is discussed below. Also shown are the approximate location of the coexistence and spinodal curves. Determination of these curves is also discussed below. The behavior of the free energy for these isotherms for all systems is more or less the same. As the reduced density increases, the free energy increases. At some mid range in reduced density the slope of the increase in free energy changes. At a greater reduced density the slope of the increase in free energy changes again. This is most clearly demonstrated by the van der Waals fluid system, see Fig. 4(d). However, the behavior is present in all the models. This behavior, while appearing modest in these plots, will be seen to be the cause of the critical-like behavior exhibited by these models.

The pressure was calculated from the free energy isotherms via Eq. (23). Figure 5 shows the results for each model. The determination of the location of the critical point and the coexistence and spinodal curves is based on the phase diagram of pressure, temperature, and reduced density. By searching for inflection points along the pressure versus

TABLE I. Critical points for the models.

System	T_c	ρ_c	P_c	C_f
V1	7.575 ± 0.005 MeV	$0.94 \pm 0.01 \times \rho_0$	$(3.2 \pm 0.1) \times 10^{-3}$ MeV/fm^3	0.49 ± 0.02
V2	6.875 ± 0.005 MeV	$0.74 \pm 0.01 \times \rho_0$	$(7.3 \pm 0.1) \times 10^{-4}$ MeV/fm^3	0.16 ± 0.02
V3	10.975 ± 0.005 MeV	$0.85 \pm 0.01 \times \rho_0$	$(2.4 \pm 0.1) \times 10^{-3}$ MeV/fm^3	0.28 ± 0.02
vdW	$1.01 \pm 0.01 \times T_c$	$1.01 \pm 0.01 \times \rho_c$	$(1.7 \pm 0.1) \times 10^{-4}$ eV/nucleon $\times V_c$	0.37 ± 0.02

reduced density isotherms the spinodal curve was determined. The isotherm immediately following, as the temperature of each isotherm increases, the last isotherm with two inflection points was labeled the critical isotherm.

Another method to determine the location of the critical point began with the isothermal compressibility which was calculated with Eq. (24). Isotherms of κ_T versus reduced density were inspected. All subcritical isotherms showed at least one negative value of κ_T. The first isotherm, as a function of increasing temperature, which showed only positive values of κ_T was labeled the critical isotherm. Both procedures yielded the same results, as they are essentially identical. See Table I.

The coexistence curve was determined by making a Maxwell equal area construction for each isotherm. See Fig. 4 for examples of the Maxwell construction.

On first glance at Table I several noteworthy features stand out. (1) None of the values of T_c determined for the models is the same as the value of the parameter T_c specified in the surface term in Eq. (4). (2) The critical densities for each model are close to unity. (3) The critical temperature of V1, the model which includes the Coulomb force, is larger than the critical temperature of V2, the model with no Coulomb force. The error of the analysis of the van der Waals fluid was on the order of a few percent; $T_c^{\text{vdW}} \neq 1$. This illustrates the error inherent with this type of analysis.

It is not surprising that the critical temperature found by the analysis of thermodynamical quantities is different than the parameter T_c used to parametrize the surface free energy of infinite nuclear matter. If one considers the critical point to be that temperature at which the surface free energy vanishes, then this can only be at T_c (16 MeV in this case). However, the form of the surface term given by Eq. (4), approximately the form of the macroscopic surface free energy of a fluid near its critical point, is not an appropriate description of the microscopic surface of a droplet [24]. Moreover, Eq. (4) leads to a specific heat which approaches negative infinity as T approaches T_c. In a more fundamental model the critical temperature would be an output of the model rather than an input. Of the phenomenological models studied here, only the van der Waals model is known to be self-consistent.

The high densities found at the critical point for V1, V2, and V3 cannot be realized if one is constrained to placing spherical nuclei without overlaps inside of the total volume. Again this issue is mentioned but not dealt with since the aim of this paper is to explore only the thermodynamical predictions of the above models.

Were this sort of model interpreted physically, the high value of the critical density determined here would suggest that the critical point could never be reached by finite nuclear matter as a multiplicity of spherical clusters at normal nuclear density could not physically fit into the critical volume. If the constraint that the breakup volume must be large enough to avoid overlapping volumes of the final state (spherical) nuclei is added, then only first order phase transitions are possible. Of course there are several problems with a strictly physical interpretation of models such as the one presented here, not the least of which is the introduction of a volume for the system. Actual nuclei excited to high energies in nucleus-nucleus collisions do not exist in a box and thus have no volume in the sense suggested here.

Item (3), the rise in T_c with the vanishing of the Coulomb force, is, on the surface, counterintuitive. Many other models of nuclear systems show just the opposite behavior [26,27]. However, those models are fundamentally different than the ones examined in this work. Such models begin by describing the free energy or chemical potential or some equivalent quantity using formulas which assume a uniform distribution of material in much the same way that the van der Waals fluid assumes a uniform density. The model in this work samples a different part of the final state phase space [25]. It will be seen that the calculation of the Coulomb term via Eq. (5) gives rise to the counterintuitive rise in the critical temperature when the Coulomb force is suppressed in the model.

To begin to understand the effect of the Coulomb energy on the critical point the same isotherm for models V1 and V2 was examined. Figures 6(a) and 6(b) show the isotherm of $T=7.2$ MeV for V1 and V2. When the coexistence curve is shown for both systems, it is obvious that for V1 the isotherm is subcritical while for V2 the isotherm is supercritical. Figures 6(c) and 6(d) begin to shed light on the cause of this counterintuitive occurrence.

For the sake of illustration, the Maxwell constructed [a line of constant slope through the coexistence region, which then leads to a constant value of the pressure through the coexistence region that will give ''equal areas'' on a pressure-volume plot, see Fig. 5(a)] path of the free energy through the coexistence region is shown as a dashed line, barely visible just below the isotherm in the coexistence region, in Fig. 6(a). The Maxwell constructed free energy is a straight line through the coexistence region. The constant slope of the Maxwell constructed free energy leads to a constant pressure for the system in the coexistence region. Because the path of Maxwell constructed free energy is very close to the path of the free energy of V1, it is difficult to see the difference in a plot such as shown in Fig. 6(a). A plot of the difference in the calculated free energy of V1 and the Maxwell constructed free energy shows what gives rise to the van der Waals loops in Fig. 5(a), see Fig. 6(c). There are
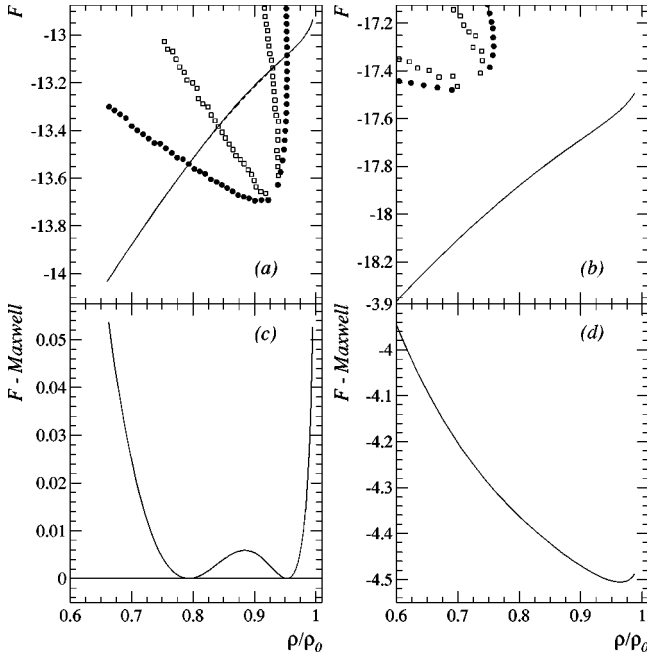
FIG. 6. Free energy isotherms as a function of reduced density for (a) V1 and (b) V2. For both systems the isotherm is for $T = 7.2$ MeV. Open squares show the spinodal, full circles show the coexistence curve. The *Maxwell constructed* free energy is shown as a dashed line through the coexistence region. The difference of the computed free energy and the *Maxwell constructed free energy* shows the presence of inflection points in (c) V1 at the coexistence boundary for this subcritical isotherm and none for (d) V2 for this supercritical isotherm.

FIG. 7. Components of the free energy isotherms ($T = 7.2$ MeV) for V1 (left) and V2 (right). From top to bottom the components are for translation, bulk or Fermi, surface, symmetry, total Coulomb, uniform background Coulomb contribution, and the clusterization Coulomb contribution.

two inflection points in the curve of the calculated free energy of V1, these are shown more clearly as the points in Fig. 6(c) where the curve shows an ordinate value of zero. These plots for a canonical system's free energy are in the same spirit as plots for a microcanonical system's entropy [28]. It is clear from Figs. 6(b) and 6(d) that there are no similar inflection points in the free energy curve for V2. Therefore the isotherm of $T = 7.2$ MeV in V2 is supercritical while the very same isotherm is subcritical for V1.

It is possible to understand what gives rise to the inflection points introduced when going from V2 to V1 by looking at the contributions to the total free energy of each system along the isotherm $T = 7.2$ MeV, see Fig. 7. Plotted in this figure for both systems are the components of the overall free energy for the isotherm in question: translational, bulk, surface, symmetry, total Coulomb, background Coulomb, and clusterization Coulomb free energies. Figure 7 shows that the translational and bulk free energies of each system are nearly identical. An inspection of Eqs. (11) and (2) shows that these quantities are relatively insensitive to small changes in the fragment distribution. On the other hand, the surface free energy shows an obvious difference in behavior between systems. In V1 the initial decrease in surface free energy as a function of reduced density is slower than in V2. An inspection of Eq. (4) shows that the $A^{2/3}$ term introduces more sensitivity to the fragment distribution than the previously discussed terms. The cause of this difference, and all the differences between these two systems, is the presence of the
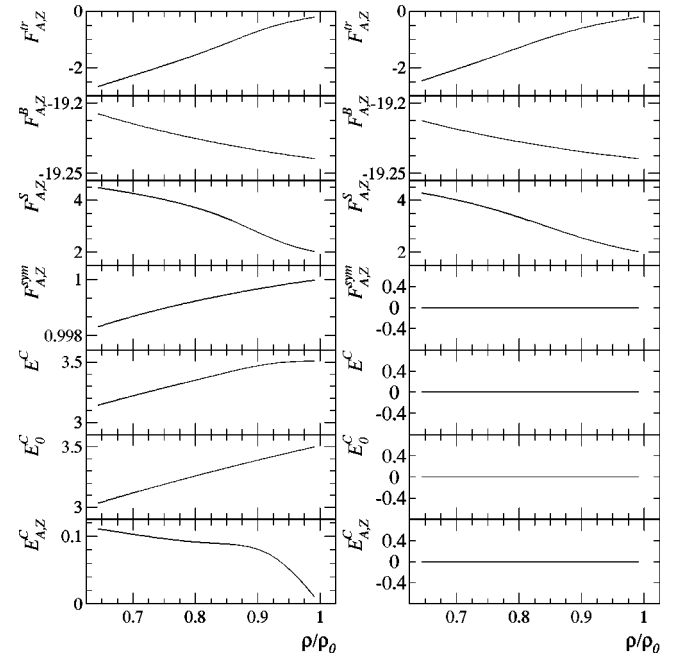
Coulomb force in V1 and its absence in V2.

The behavior of the Coulomb contribution to the free energy of this isotherm is now discussed. The first, and simplest, additional term in the free energy due to the Coulomb force is the asymmetry term. The change is in the asymmetry term is smooth as a function of increasing density and will not introduce the inflection points in the free energy curve that will change a supercritical isotherm to a subcritical isotherm.

In this model the total Coulomb contribution to the free energy comes from two sources. One which represents the background energy due to a uniform distribution of charges, Eq. (13), and the other due to the energy from the clusterization of fragments, Eq. (5) [1]. The background energy, E_0^c, goes as $\rho^{1/3}$ and therefore varies smoothly with volume. The clusterization free energy $E_{A,Z}^{C}$ shown in Fig. 7 has a different behavior. It decreases as the reduced density increases, the rate of decrease is at first nearly constant, then slows and then increases rapidly over some small interval in reduced density. The combination of these two Coulomb terms introduces sufficient changes in the overall free energy of the system from V2 to V1 that inflection points arise and thus the critical temperature increases when the Coulomb force is added to the system. A smooth or constant version of the Coulomb free energy added to version V2 should not cause this sort of behavior. It is the variation in $E_{A,Z}^{C}$ that introduced the inflection points and increases the critical temperature. In the end, it is the behavior of the free energy curve that served to determine the location of the critical point and that behavior is, at times, counterintuitive.
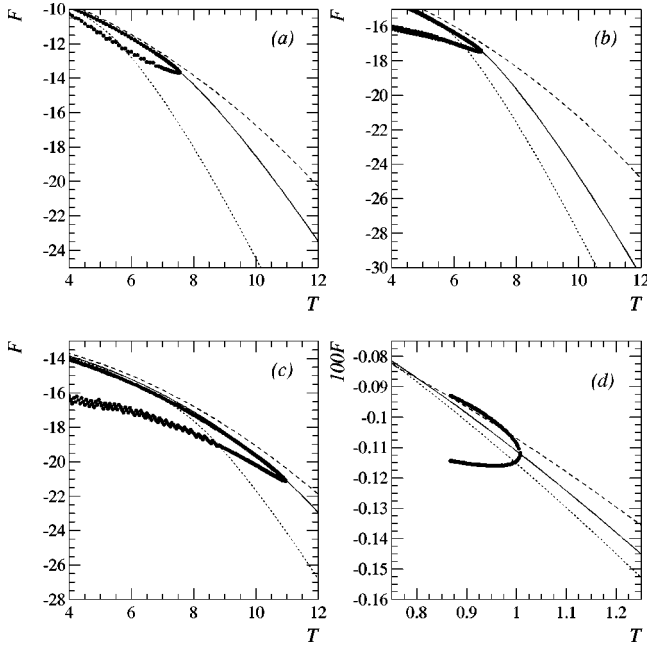
FIG. 8. Free energy isochores for (a) V1, (b) V2, (c) V3, and (d) the van der Waals fluid. Full circles show the boundary of the coexistence region. Dotted curves are subcritical. Solid curves are critical. Dashed curves are supercritical.
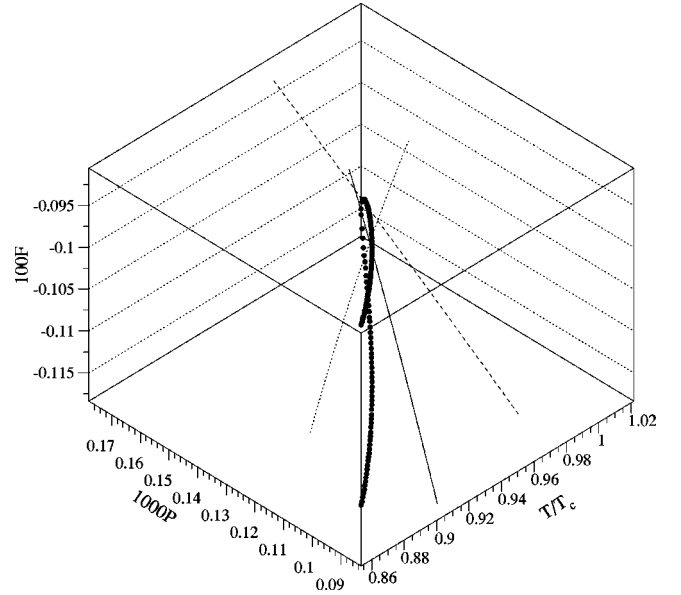

FIG. 9. A three-dimensional plot of the free energy isochores for the van der Waals fluid. Full circles show the boundary of the coexistence region. Dotted curves are subcritical. Solid curves are critical. Dashed curves are supercritical.

Also listed in Table I is the compressibility factor:

$$C_f = \frac{P_c V_c}{T_c}. \qquad (25)$$

The textbook value for C_f for the van der Waals gas is recovered to within error bars. According to the law of corresponding states, the value of C_f should be universal. For fluid systems this is the case and $\langle C_f \rangle \sim 0.292$ [29]. For V1 and V2 no such universal behavior is observed to within error bars, while V3 shows some degree of universality.

B. Isochores

The volume of the system is held constant and the behavior of various quantities with respect to the system's temperature is explored.

Beginning again with the primary quantity calculated, Fig. 8 shows the free energy for each system as a function of the system's temperature. For models V1, V2, and V3 the isochores are for $\rho = \rho_0/3$, $\rho = \rho_c$, and $\rho = 0.9995\rho_0$. For the van der Waals fluid, the isochores shown are for $\rho = 1.25\rho_c$, $\rho = \rho_c$, and $\rho = 0.75\rho_c$. See Table I for critical density values. Also shown are the values of the free energy of the systems along their respective coexistence curves.

In Ref. [8] the authors show results of a model similar to V2, for an isochore of approximately $\rho = \rho_0/3$. In that work there was a *kink* in the free energy curve which was interpreted as evidence for a first order phase transition. For the small system used in this work the *kink* is smoothed out negating the efficacy in using the kink as evidence towards determining the order of a phase transition if one is present. In larger systems, systems in Ref. [8] were more than 15

times larger than the system used in this work, the kink is more evident and this procedure may be possible.

Knowledge of the location of the coexistence curve allows for the identification of subcritical, critical, and supercritical isochores. For the projections shown in Fig. 8 all the versions of the nuclear model have a subcritical isochore that crosses the coexistence region. The critical isochore travels along the high value edge of the coexistence curve passing through the critical point. Supercritical isochores do not come into contact with the coexistence curve nor do they traverse the coexistence region. The behavior of the van der Waals fluid is somewhat different from the behavior of the nuclear models. Figure 8(d) shows that for a van der Waals fluid in this projection of the phase diagram all isochores are in the coexistence region for low temperatures and cross the coexistence curve at higher temperatures. This apparent behavior results from projection of the three dimensional phase diagram onto a two-dimensional plot. In a three-dimensional figure, the supercritical isochore is seen to travel outside the coexistence region, the critical isochore is observed to intersect with the critical point and the subcritical isochore is seen to traverse the coexistence region, see Fig. 9.

The pressure isochores were obtained by following the procedure outlined in Eq. (23) and using $\langle \rho \rangle$, the average density, and $\langle T \rangle$, the average temperature over the ΔT interval, see Fig. 10. In the limit of vanishing ΔT this procedure is valid. Figure 10 shows the same three isochores discussed above as well as the location of the coexistence curve, seen edge on in this projection of the phase diagram. All the figures for the nuclear model show similar behaviors for the critical and supercritical isochore. All supercritical isochores follow a trajectory above the coexistence curve. The critical isochore for all versions of the model approaches the coexistence curve, follows it, and leaves at the termination or
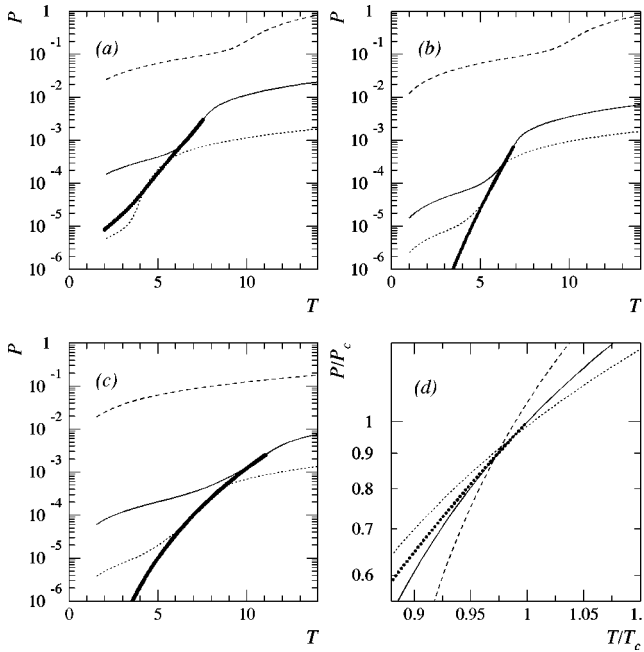
FIG. 10. Isochores of pressure versus temperature for (a) V1, (b) V2, (c) V3, and (d) the van der Waals fluid. Full circles show the boundary of the coexistence region. Dotted curves are subcritical. Solid curves are critical. Dashed curves are supercritical.
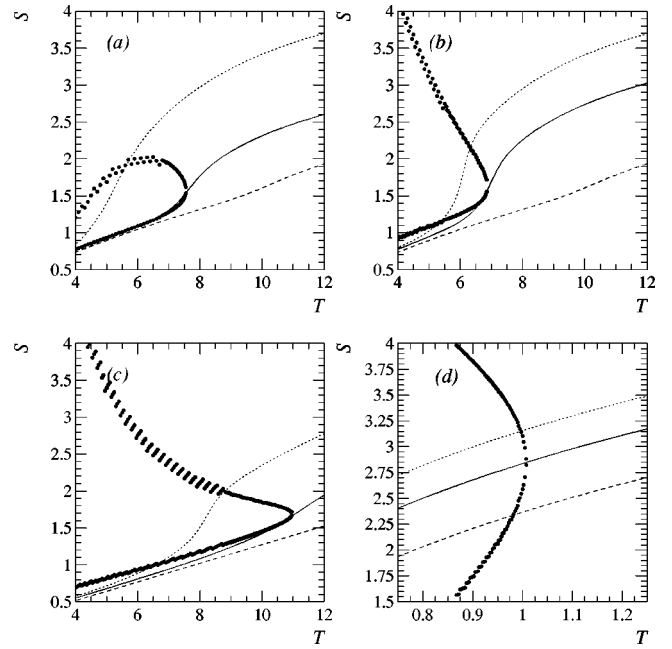

FIG. 11. Isochores of the entropy versus temperature for (a) V1, (b) V2, (c) V3, and (d) the van der Waals fluid. Full circles show the boundary of the coexistence region. Dotted curves are subcritical. Solid curves are critical. Dashed curves are supercritical.

critical point. The subcritical isochores for V2 and V3 pass through the coexistence curve as the temperature is increased and the system makes a first order transition from a liquid to gaseous state. For version V1 the behavior is more complicated. The subcritical isochore begins on the gaseous side of the coexistence curve, crosses the coexistence curve into the liquid region before crossing back over the coexistence curve into the gaseous region at higher temperature. The P-T projection of the van der Waals fluid looks as expected, see Fig. 10(d).

Following the analysis procedure outlined in the previous section, the entropy was determined via Eq. (20), see Fig. 11. The same three isochores are plotted showing the entropy as a function of temperature. All three isochores for the nuclear models show a smooth rise as a function of temperature with some region of increased slope. This behavior is consistent with a continuous phase transition, if a phase transition were present. Along an isochore, a first order transition would be indicated by a sudden change the behavior of the entropy as a function of temperature at one edge of the coexistence region. However, due to the small size of the system such sharp behavior is smoothed making it impossible to come to a conclusion about the order of a phase transition from plots such as those shown in Fig. 11. As before, knowing the location of the coexistence curves makes identification subcritical, critical, and supercritical isochores a trivial matter. The subcritical isochore traverses the coexistence region, the critical isochore passes through the critical point and the supercritical isochore avoids the coexistence region. As before the van der Waals system shows a different behavior, and a dimension to the plot in Fig. 11(d) must be added to understand the behavior of the various isochores.

The specific heat at a constant volume C_V for each system is shown in Fig. 12, again for the same three isochores. All curves show a peak that could be due to a smoothed out discontinuity (first order phase transition), the remnants of a power law divergence at the critical point (continuous phase
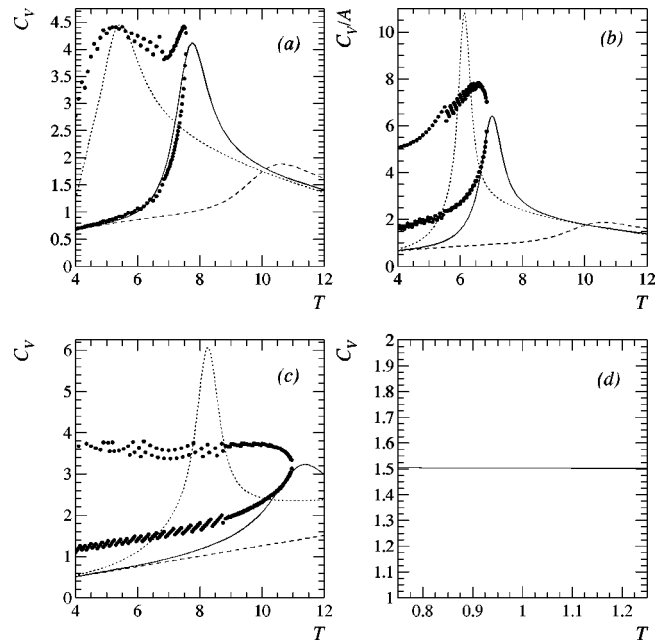

FIG. 12. The specific heat at constant volume versus temperature for (a) V1, (b) V2, (c) V3, and (d) the van der Waals fluid. Full circles show the boundary of the coexistence region. Dotted curves are subcritical. Solid curves are critical. Dashed curves are supercritical.
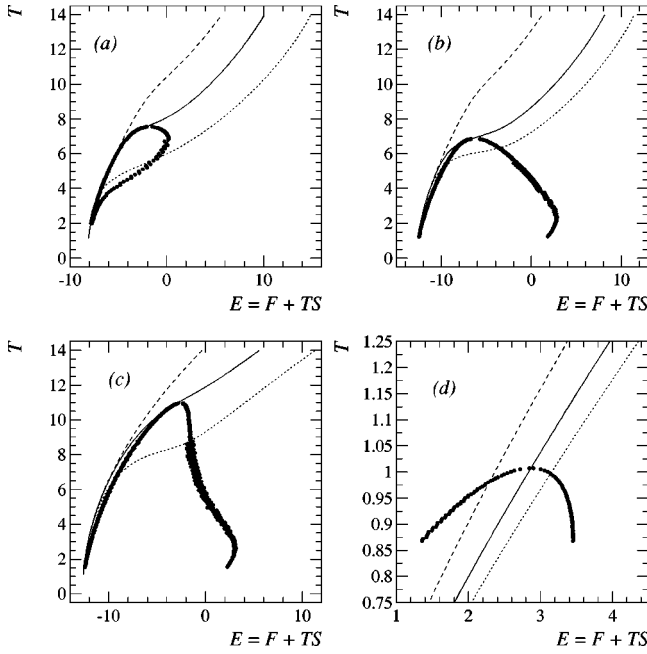
FIG. 13. Isochoric caloric curves for (a) V1, (b) V2, (c) V3, and (d) the van der Waals fluid. Full circles show the boundary of the coexistence region. Dotted curves are subcritical. Solid curves are critical. Dashed curves are supercritical.
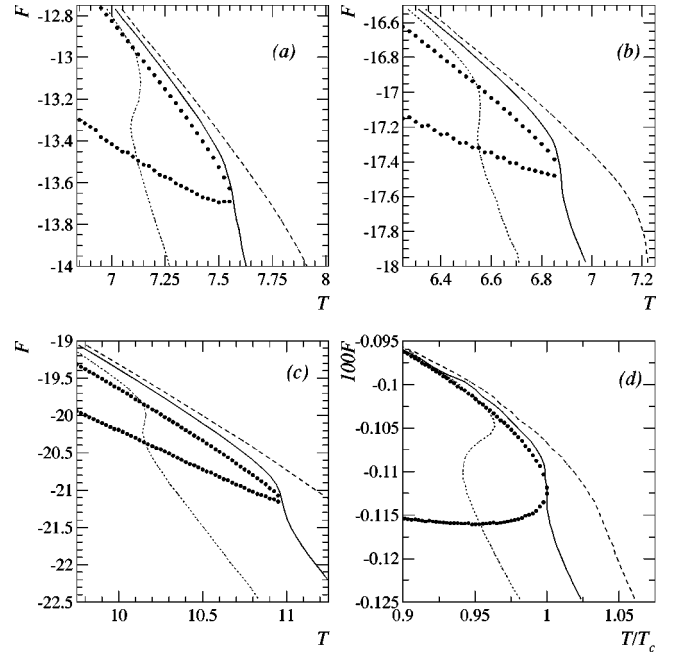

FIG. 14. Free energy isobars as a function of the temperature for (a) V1, (b) V2, (c) V3, and (d) the van der Waals fluid. Full circles show the boundary of the coexistence region. Dotted curves are subcritical. Solid curves are critical. Dashed curves are supercritical.

transition) or a specific heat anomaly (supercritical behavior). As with the free energy and entropy it is impossible to come to a definite conclusion regarding the presence and nature of a phase transition from this plot. Of particular importance is the specific heat for the van der Waals fluid which is seen to be nearly constant and equal to 3/2 as it should [30]. There is a small slope for the specific heat over the temperature range in question: for $T=T_c/2$ $C_V=1.507$ and for $T=2T_c$ $C_V=1.502$. This illustrates the technique employed here, following Eqs. (20) and (21), yields results that are no better than 0.25% for the quantities determined in this paper.

Finally, Fig. 13 shows the constant volume caloric curves of T as a function of E for each system at the same isochores discussed above. Also shown are the values of the temperature and energy of the system, $E=F+TS$, along the boundary of the coexistence region. Just as with the behavior of the entropy isochores, the behavior of the caloric curves for each isochore shows behavior that is consistent with either a first order or continuous phase transition in a small system. Each isochore shows similar behavior, a steep rise followed by a region of shallower incline followed by a portion which approaches $E/A=\frac{3}{2}T$. The lack of a flat region, or back bend, in the caloric curve is not due to the small size of the system but rather due to the system being held at a constant volume. Only for *isobars* will flat regions or back bends be observed in the canonical nuclear model (see the following section). Again the van der Waals system shows very different behavior, a steady rise in the temperature as a function of energy. And again a three dimensional plot is needed to clearly understand the nature of each isochore.

C. Isobars

The pressure of the system is held constant and the behavior of various quantities with respect to the system's temperature is explored. Here some care should be taken with the interpretation of the results. The analysis outlined above is still followed. However, since the pressure is an extensive quantity, plots such as free energy versus temperature are now plots of $\langle F \rangle$ versus T. Where $\langle F \rangle$ is the mid point in the ΔF range over which a difference such as Eq. (23) is taken. In the limit of vanishing interval size, this approximation is accurate. Also because the pressure is an extensive variable, it was necessary to allow some small variation in P in order to make a plot such as $\langle F \rangle$ against T. The variation in P was usually less than one percent; i.e., $\Delta P/P \leq 0.01$. Small changes in the amount of variation of P had little effect on the analysis presented here. Large changes in the variation in P wash out the behavior observed below.

The isobaric free energy as a function of temperature is shown for all systems in Fig. 14 as well as the values of the isobaric free energy along the boundaries of the coexistence region. In all systems there is a back bend in the free energy curve for subcritical isobars. The subcritical isobar also traverses the coexistence region. It would be possible to perform the Maxwell construction procedure and deduce the critical point from these plots. The van der Waals fluid system shows that the critical point determined in the construction of the P-V coexistence curves agrees with considerations of isobaric F, see Fig. 14(d). The critical isobar shows a vertical slope tangent to the coexistence curve and no back bend. The supercritical isobar does not traverse the coexistence region and shows no back bend.
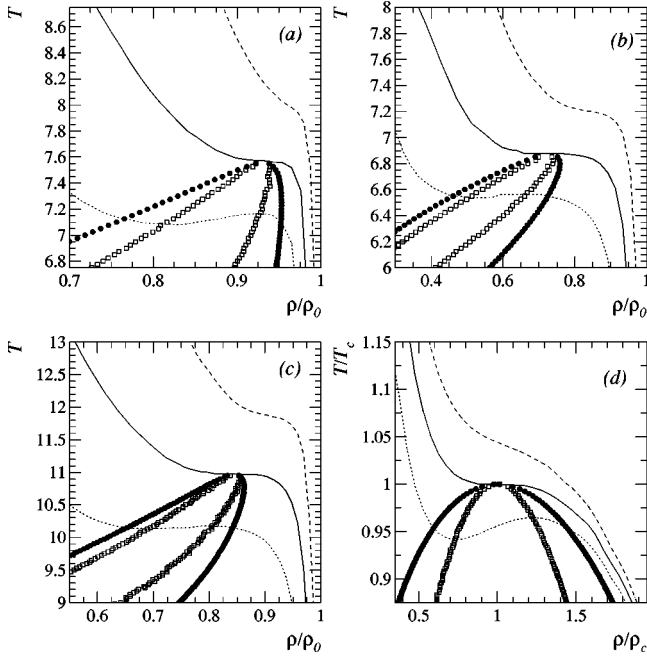
FIG. 15. Isobars of temperature versus reduced density for (a) V1, (b) V2, (c) V3, and (d) the van der Waals fluid. Open squares show the spinodal. Full circles show the boundary of the coexistence region. Dotted curves are subcritical. Solid curves are critical. Dashed curves are supercritical.

Figure 15 shows the isobaric temperature as a function of reduced density. Temperature is plotted as a function of reduced density in the spirit of the Guggenheim plot [31] which shows the universal behavior of several fluids near their critical point. On the scales shown here no universal behavior is observed. It may be that very near the critical point, the coexistence curves for each system are identical. The T-ρ isobars for all systems show the expected behaviors: a subcritical back bending curve that traverses the coexistence region giving way to the critical isobar, a critical curve with a flat section which intercepts the coexistence region at the critical point and finally a supercritical isobar which avoids the coexistence region altogether.

The behavior of the isobaric entropy as a function of temperature is also just as expected, see Fig. 16. Figure 17 shows the isobaric caloric curves for each system. As the energy is constructed from the free energy and entropy of the system the back bending observed in the subcritical isobars is expected. Also shown is the value of temperature and energy along the boundary of the coexistence region. Note the difference between the isochoric caloric curves shown in Fig. 13 and the isobaric caloric curves shown in Fig. 17. When the pressure is held constant all of the canonical systems discussed here, including the van der Waals fluid, show subcritical caloric curves with a back bend. No back bending is present when the volume is held constant.

Finally Fig. 18 shows the constant pressure specific heat, C_P, as calculated from

$$C_P = \left(\frac{\Delta E}{\Delta T} \right)_P \qquad (26)$$
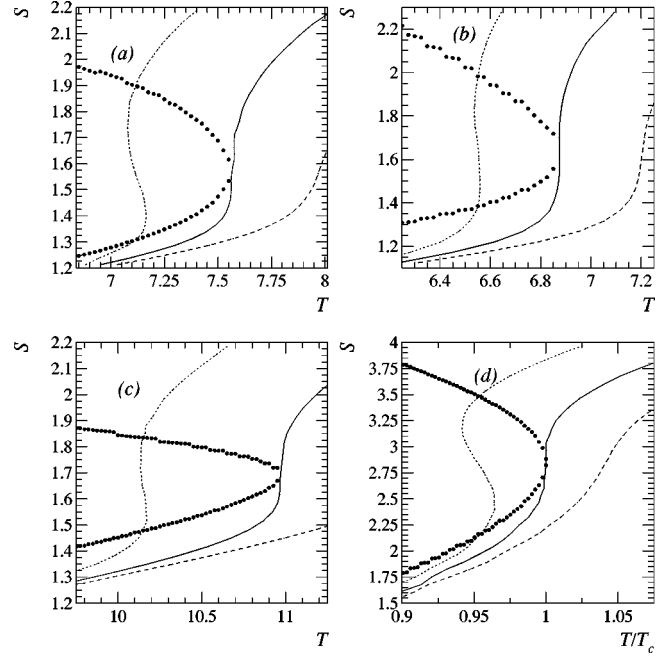

FIG. 16. Isobars of the entropy versus temperature for (a) V1, (b) V2, (c) V3, and (d) the van der Waals fluid. Full circles show the boundary of the coexistence region. Dotted curves are subcritical. Solid curves are critical. Dashed curves are supercritical.

taking as input the isobars shown in Fig. 17. The results for C_P of these canonical calculations are similar to the behavior reported in microcanonical models for various systems [2,28,32,33]. The subcritical isobars show the remnants of poles with $C_P < 0$ values in between. The critical isobar shows the remnants of a divergence, and the supercritical isobar shows some peaking behavior. The lack of poles and divergences is not due to the finite size of the systems V1, V2, and V3, but rather due to the computational nature of these calculations. The calculations for the van der Waals fluid are, in effect, for a truly thermodynamic system and the van der Waals critical isobar of C_P still shows no true divergence. The critical isobar of C_P for V2 shows a negative value which is due to the computational nature of the calculation and the manner in which C_P was calculated from E and T values.

D. Isonothing: Variable (P,V,T)

The nuclear model presented here assumes a system enclosed in some volume. An actual excited nucleus is not enclosed in a volume. This has the effect of forcing a path through the thermodynamic phase space which is considerably different from any of the paths investigated thus far. To bridge the gap between reality and tractable calculations, an energy dependent free volume is assumed in models such as the ones presented in this work [1]. At low energies the free volume of the system is assumed to be nearly constant and vanishingly small. At a given energy the system is allowed to expand and the free volume increases from near zero. This has the effect of tracing a path through the thermodynamic phase space of the system off any of the trivial paths along
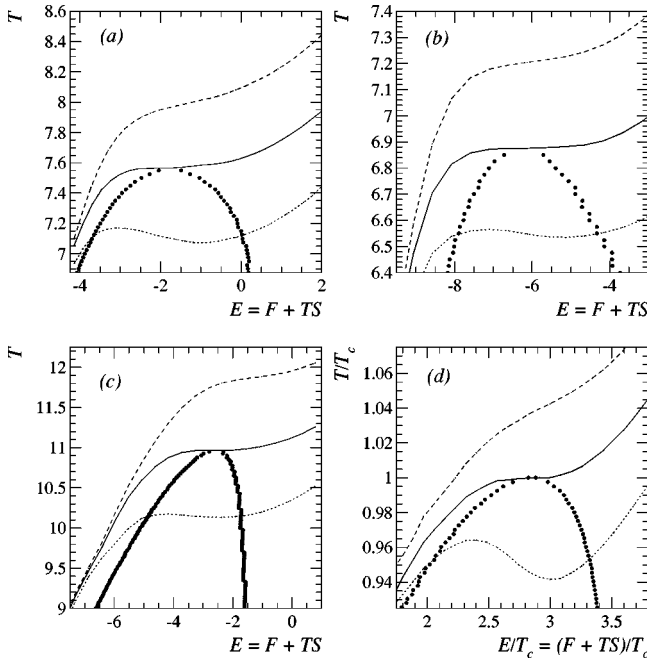
FIG. 17. Isobaric caloric curves for (a) V1, (b) V2, (c) V3, and (d) the van der Waals fluid. Full circles show the boundary of the coexistence region. Dotted curves are subcritical. Solid curves are critical. Dashed curves are supercritical.

one of the axes investigated above. It is possible to examine the effects of such a parameterization of the free volume as a function of energy with the calculations made here. Calculations in this section were performed only for V1.

Following the same ideas presented in the discussion of isobars, the values of F, S, and T are determined along a path
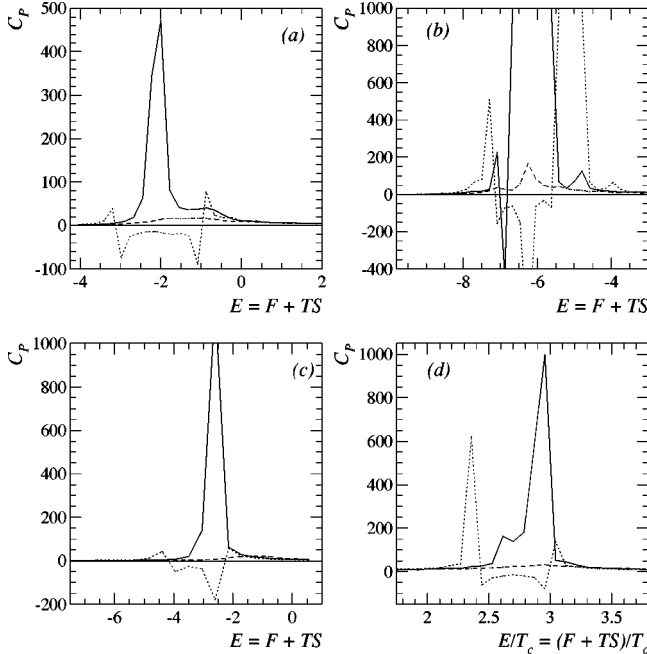

FIG. 18. Specific heat at a constant pressure versus energy for (a) V1, (b) V2, (c) V3, and (d) the van der Waals fluid. Dotted curves are subcritical. Solid curves are critical. Dashed curves are supercritical.
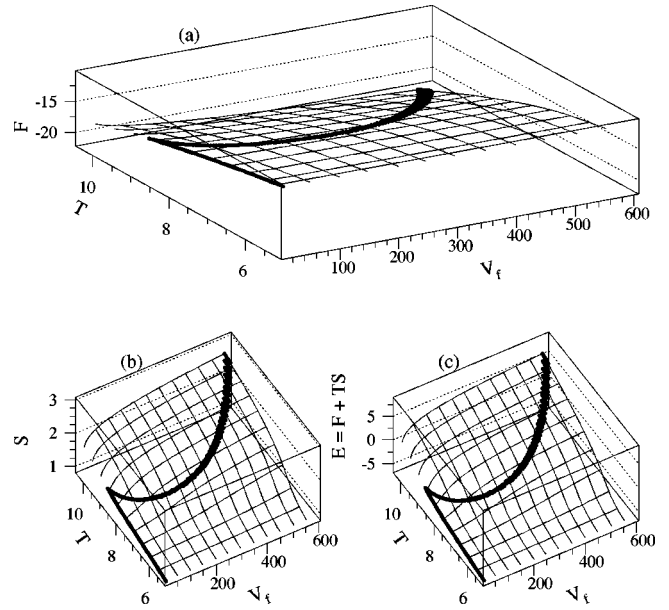

FIG. 19. Solid circles show the path of an expanding nuclear system V1 through thermodynamic phase space. Neither volume nor pressure is held fixed. Points show the calculations of the free energy surface as shown in Fig. 3.

in V_f as a function of E. As V_f changes values of F, S, and E are picked from the appropriate isochore. For example, instead of traveling along a path parallel to one of the axes in Fig. 2(a), e.g., an isochore, isotherm, or isobar, an energy-dependent free volume was chosen so that the system evolved through thermodynamic phase space on a nontrivial trajectory, see Fig. 19. In Fig. 19(a) small points show a small sample of the set of calculations for $F(T,V)$. Larger points show the values of $F(V,T)$ selected for a $V_f(E)$ trajectory described above. Figures 19(b) and 19(c) show the same for $S(T,V)$ and $E(T,V)$.

For the purposes of the present analysis, values of $S(T,V)$ were used from different isochores. As V_f changed values of $S(T,V)$ were selected from the appropriate isochore. If the change from isochore to isochore is small, $\Delta V_f \sim 0$, then the procedure is a good approximation. The intervals in V_f for the calculation of $F(T,V)$ for this analysis were on the order of two percent of the free volume of the system; e.g., when $V_F = 500$ fm^3, $\Delta V_f \sim 10$ fm^3, and when $V_f = 5$ fm^3, $\Delta V_f \sim 0.1$ fm^3.

Figure 20(a) shows three different paths through thermodynamic phase space: one which travels very near to the critical point and into the coexistence region (solid curve), and two others which avoid the coexistence region all together (dotted and dashed curves). As mentioned previously for the full version of this model [1] the free volume is nearly zero for the lower end of the energy range. At some energy, 2 MeV/nucleon for the solid curve in Fig. 20, the system is allowed to expand and the free volume increases as a function of energy. The functional form of $V_f(E)$ is not identical to other models [1] but close enough to show the same behavior observed in the full version of the model [1]. Also shown in Fig. 20(a) are the values of the free volume
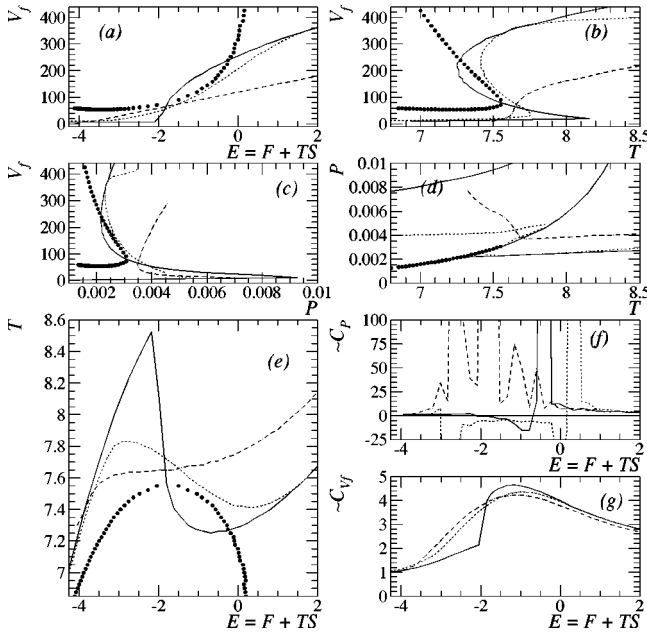
FIG. 20. The path of an expanding nuclear system V1 through thermodynamic phase space: (a) the free volume as a function of energy, (b) free volume as function of temperature, (c) free volume as a function of pressure, (d) pressure as function of temperature, (e) the resulting caloric curve, (f) a specific heat based on the derivative of the caloric curve, and (g) a specific heat along the phase space trajectory. Full circles show the boundary for the coexistence region. Different line types show different (P, V, T) trajectories. See text for details.

and energy along the boundary of the coexistence region. Note that for the solid curve the $V_f(E)$ trajectory enters the coexistence region near the critical point and leaves the coexistence region at a higher energy and free volume. The other two trajectories shown in Fig. 20 have the same general behavior: increasing free volume with increasing energy, but the precise paths differ.

In a plot of free volume against temperature back bending is observed for two of the trajectories presented here, see Fig. 20(b). The solid curve trajectory of $V_f(T)$ begins with a small free volume that is constant until a temperature of just over 8 MeV, then the system expands and cools. This is shown by the back bend. The solid curve $V_f(T)$ trajectory then enters the coexistence region near the critical point. At a temperature between 7 and 7.5 MeV the slope of the free volume nearly diverges and then changes in sign. After this point, further expansion in the free volume is accompanied by an increase in the temperature of the system. The $V_f(T)$ curve then leaves the coexistence region at $T < T_c$ and $V > V_c$. The other trajectories show similar, but less extreme behavior.

Other projections of the phase diagram for this model with the solid curve $V_f(E)$ trajectory show back bends as well, see Figs. 20(c) and 20(d). The V_f-P projections shows the system's pressure increases nearly an order of magnitude over the constant free volume section. When the system is allowed to expand, the pressure drops. The trajectory passes near the critical point as it enters the coexistence region and

in the course of back bending exits the coexistence region.

The solid curve P-T trajectory is equally interesting. As the system increases in temperature with a fixed free volume, the pressure increases. When the system reaches a temperature between 8 and 8.5 MeV the expansion sets in and the pressure and temperature both drop so that the trajectory moves towards the critical point. At a temperature between 7 and 7.5 MeV, the system reverses the trend and both pressure and temperature increase, see Fig. 20(d). Again the other two trajectories show similar behavior, but to a lesser extent as the $V_f(E)$ trajectory becomes smoother.

As back bending has already been observed for other $V_f(E)$ trajectories, it is no surprise that the caloric curve for this changing volume system also shows a back bend, see Fig. 20(e). The solid caloric curve shown here is reminiscent of other back bending caloric curves already published in Refs. [1,20–22], where variable free volume constrained canonical and constrained grand canonical calculations are made, but not those published in Refs. [2,28], where a constant volume micro canonical calculation is made. Also shown in Fig. 20(e) are the values of the temperature and energy along the coexistence curve. Again the trajectory of the solid curve variable free volume enters the coexistence region near the critical point and exits the coexistence region at $T < T_C$ and $E > E_c$. The dotted caloric curve also shows back bending, albeit to a more limited extent and the dashed caloric curves shows no major back bend.

Next the specific heat of the system was calculated via Eq. (26), see Fig. 20(f). The application of Eq. (26) to this trajectory through thermodynamic phase space is problematic. From Fig. 20(d) it is clear that pressure is not a constant and thus Eq. (26) should not be used. However, it has become commonplace to follow this sort of procedure [20,22], even though it is in contradiction with definition of C_P or C_V. When Eq. (26) is applied to the solid and dotted curves in Fig. 20(e), the resulting specific heat shows negative values and the remnants of a divergence.

Finally the specific heat of the system was determined in the same manner that the entropy of the system was determined. The specific heat at a constant volume was calculated along an isochore, then the values of C_V were selected from the paths through thermodynamic phase space of the $V_f(E)$ trajectory, see Fig. 20(g). For the solid line path, the value of C_V shows a steady rise until an energy of 2 MeV/nucleon and then a sharp rise as the system expands. As the system continues to expand and the energy increases the value of C_V reaches a maximum and then shows a gradual decline. No $C_V < 0$ is observed in this plot. The other two paths show smoother behavior.

The question that now arises is what, if any, insight into the nature of the phase transition can be obtained from curves such as those in Figs. 20(e) and 20(f). Were there no other knowledge of the system, the back bends observed in the solid and dotted caloric curves would suggest that the system had gone through a first order phase transition. Negative values and a peak in the specific heat would seem to confirm this. While for the dashed curve, the lack of back bending in the caloric curve and the lack of a negative specific heat would argue either for a continuous phase transi-

tion or no phase transition. However, from the analysis of the previous sections, the location of the critical point and the shape and location of the coexistence curve are known. The addition of this knowledge makes it clear that the naive analysis of Figs. 20(e) and 20(f) can provide misleading results. While the solid caloric curve shows a back bend, the trajectory of the systems goes through the critical point, into the coexistence region and exits along a subcritical path. Can one conclude that the system has undergone a continuous phase transition, or has it undergone a first order phase transition because the trajectory traverses the coexistence region? The answer to the first question is yes, since the system does reach the critical temperature and density simultaneously. The answer to the second question also appears to be ''yes'' since the specific heat found from Eq. (26) is less than zero (for the solid curve). Furthermore, the solid curve intersects the coexistence curve at a T less than T_c. Note, however, that without knowledge of the location of the coexistence curve, the above questions cannot be unambiguously answered. A naive inspection of the dotted caloric curve may lead one to conclude that the back bending is indicative of a first order phase transition. Such is not the case, Fig. 20(e) shows that the dashed line never traverses the coexistence region. It is clear that drawing conclusions based on caloric curves is difficult unless one has knowledge of the complete thermodynamics of the system.

E. Critical exponents from thermodynamic quantities

Any model that attempts to describe a system capable of undergoing a continuous phase transition should exhibit quantities with singular behavior that, near the critical point, are described by power laws with a consistent set of critical exponents. These critical exponents should obey well known scaling laws and may, or may not, fall into one of the established universality classes. To that end, five critical exponent values are determined and four scaling laws are checked for these models using the critical point (T_c, P_c, ρ_c) determined previously and other thermodynamic quantities. Note that in the determination of critical exponents presented here, thermodynamic variables are used explicitly, e.g., in the extraction of γ it is the isothermal compressibility that is used, and not moments of the fragment distribution.

1. Power law results

The exponent α is determined by the behavior of the specific heat along the critical isochore, see Fig. 12. The $C_V(T)$ curve was fit with the functional form

$$C_V(T) = H_\pm \left(\frac{\left| \frac{T-T_c}{T_c} \right|^{-\alpha_\pm} - 1}{\alpha_\pm} \right) + G_\pm \qquad (27)$$

on both sides of the critical point $T \gtrless T_c$ [34]. The fit parameters $H_\pm$, $\alpha_\pm$, and $G_\pm$ were allowed to vary to minimize the χ^2 of the fit. Figure 21 shows the results for each system and Table II lists the extracted exponents.

The functional form in Eq. (27) did not fit the curves shown in Figs. 21(a), 21(b), and 21(c) over the entire range
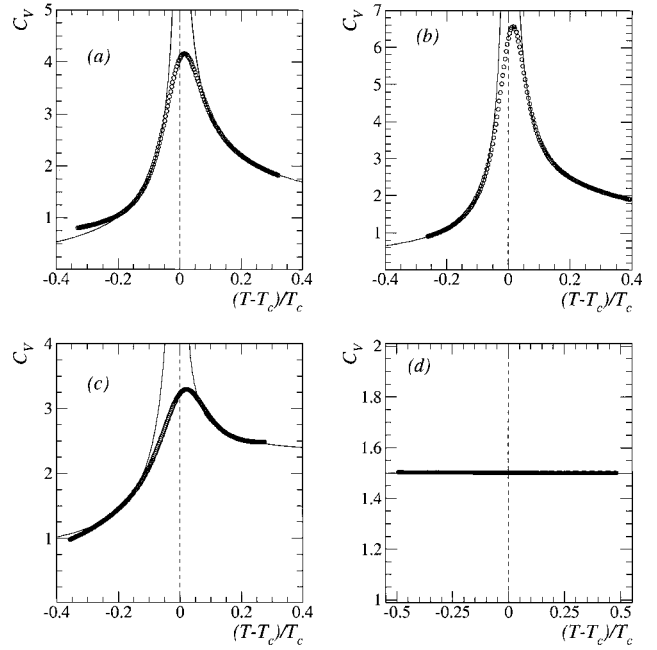

FIG. 21. Determination of the critical exponent α from the specific heat at a constant density $\rho = \rho_c$ for (a) V1, (b) V2, (c) V3, and (d) the van der Waals fluid. Solid lines show a sample fit.

of $(T-T_c)/T_c$. To some degree this is to be expected. Near the critical point the finite size effects, which manifest themselves first in the smoothing of the kink of subcritical free energy isochores, diminish a diverging specific heat into a peaking specific heat. Far from the critical point, the analytic terms in the expression for the specific heat become dominant and the power law behavior is overwhelmed. In some midrange region, neither too far from nor too near to the critical point behavior consistent with Eq. (27) was observed. Various fits were tried on both sides of the critical point, but only those which gave a matching value for α were considered. Figures 21(a), 21(b), and 21(c) show the results of one such fit. Table II lists the average results for many such fits.

The van der Waals fluid shows much different behavior that do the nuclear models. The constant value of $C_V = 3/2$ in the van der Waals fluid leads to the result of $\alpha = 0$ as expected for a mean field model. Based on this result it would seem that the nuclear models are not mean field models. They show a peaking in the specific heat that is inconsistent with the behavior of a van der Waals fluid type of mean field model or the behavior of the Landau model which shows a discontinuity in the specific heat.

The exponent β is determined using the (P, V_f) points along the coexistence curve, shown in Fig. 15, which should be described by

$$\rho_l - \rho_g \sim \left(\frac{T_c - T}{T_c} \right)^\beta. \qquad (28)$$

Fitting $\rho_l - \rho_g$ versus $(T-T_c)/T_c$ to a simple power law for the positive slope portion of Figs. 22(a), 22(b), and 22(c) gives the exponent β, see Table II for results. The van der

TABLE II. Critical exponents for the models.

System	$\alpha_\pm$	β	γ	δ_+	δ_+	τ
V1	0.6 ± 0.2	0.5 ± 0.2	1.0 ± 0.2	1.2 ± 0.3	1.4 ± 0.3	2.49 ± 0.03
V2	0.9 ± 0.2	0.6 ± 0.1	1.0 ± 0.4	2.8 ± 0.1	2.7 ± 0.2	2.10 ± 0.02
V3	1.0 ± 0.2	0.8 ± 0.1	1.2 ± 0.2	2.5 ± 0.2	3.2 ± 0.2	2.22 ± 0.02
vdW	0.0	0.5 ± 0.1	0.98 ± 0.02	2.7 ± 0.2	3.1 ± 0.3	2.33 ± 0.02

Waals fluid recovers the mean field value of $\beta = 1/2$. The model V1 gives the least impressive fit results.

Near the critical point the isothermal compressibility κ_T, is given by

$$\kappa_T = \Gamma_\pm \left| \frac{T - T_c}{T_c} \right|^{\gamma_\pm}. \tag{29}$$

For $T < T_c$ fitting κ_T versus $|(T - T_c)/T_c|$ along the coexistence curve gives γ_- while γ_+ is determined by fitting κ_T versus $|(T - T_c)/T_c|$ for $T > T_c$ at $\rho = \rho_c$. Due to the imprecise nature of the data along the coexistence curve for $T < T_c$ fits were made only for $T > T_c$. Fits were made over the entire region of $|(T - T_c)/T_c|$ of $T > T_c$. The results for the extraction of the exponent γ are shown in Fig. 23.

For V1 two different power law regions appear to be present, one close to the critical point and one further from the critical point, see Fig. 23(a). The error bars on the γ value in Table II account for this behavior. The fit to the entire $|(T - T_c)/T_c|$ region is used because the resulting power law shows some agreement with the behavior of κ_T for $T < T_c$ when the coefficient of the power law is increased

by some factor. See the dashed line and open squares in Fig. 23(a). Similar arguments apply to the results for V2 and V3, see Figs. 21(b) and 21(c).

The van der Waals fluid shows the expected behavior and recovers the value of $\gamma = 1$ to within error bars, see Fig. 23(d) and Table II for results. The $T < T_c$ behavior of κ_T also shows the expected power law behavior with the appropriate exponent value.

Examining the shape of the critical isotherm leads to an estimation of the exponent δ from

$$|P - P_c| \sim \left| \frac{\rho - \rho_c}{\rho_c} \right|^{\delta_\pm}. \tag{30}$$

The critical isotherm was examined independently for $\rho < \rho_c$, which gives δ_-, and $\rho > \rho_c$, which gives δ_+. As with the exponents α and γ, a system with a continuous phase transition the values of $\delta_\pm$ should be the same on both sides
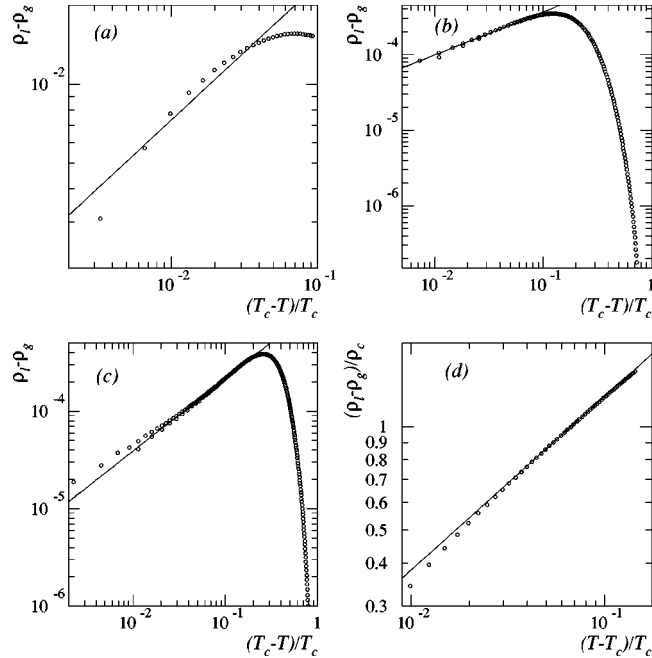

FIG. 22. Determination of the critical exponent β from the liquid-gas density difference along the coexistence curve for (a) V1, (b) V2, (c) V3, and (d) the van der Waals fluid. Solid lines show a sample fit.
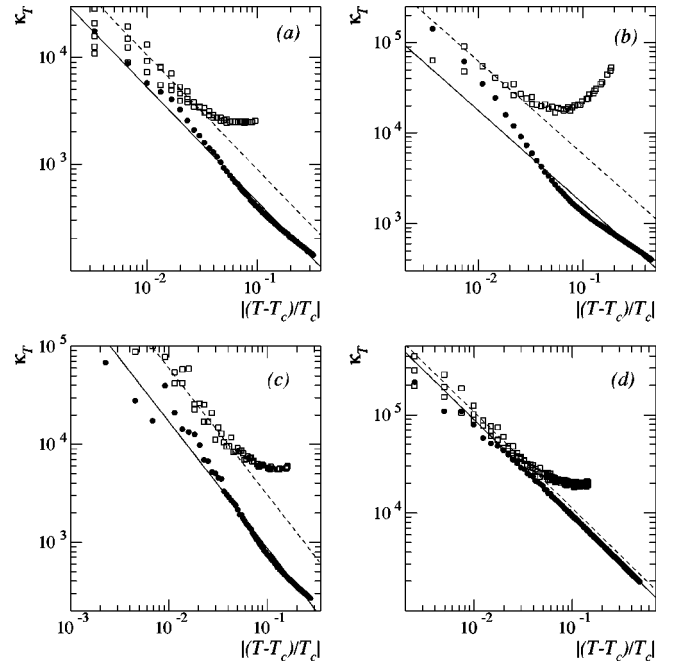

FIG. 23. Determination of the critical exponent γ from the isothermal compressibility κ_T for (a) V1, (b) V2, (c) V3, and (d) the van der Waals fluid. Solid circles show the behavior of κ_T for $T > T_c$ and at $\rho = \rho_c$. Solid lines show a sample fit. Open squares show the behavior of κ_T along one edge of the coexistence boundary. Dashed lines show the fit for $T > T_c$ multiplied by a constant.
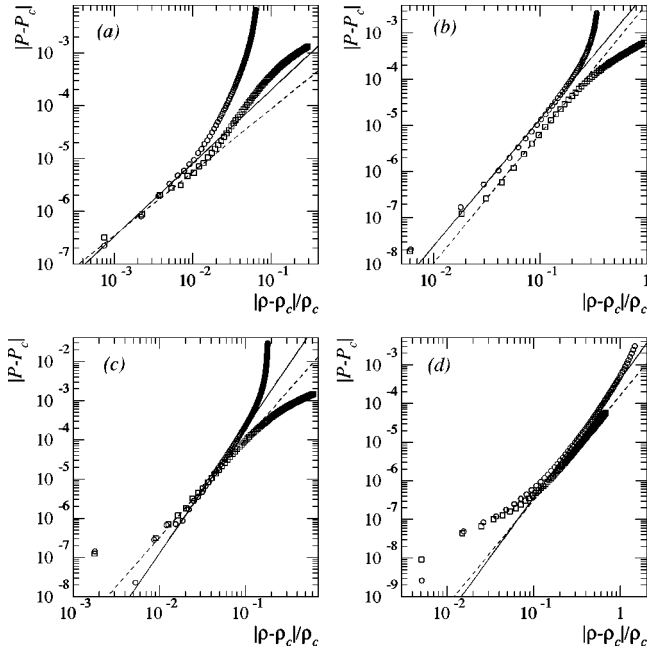
FIG. 24. Determination of the critical exponent δ from the critical isotherm for (a) V1, (b) V2, (c) V3, and (d) the van der Waals fluid. Open circles show the critical isotherm for $\rho > \rho_c$. Solid lines show a sample fit. Open squares show the critical isotherm for $\rho < \rho_c$. Dashed lines show a sample fit.

of the critical density. This fact is again used as guide in searching for fitting regions to extract the exponent δ, see Fig. 24 and Table II.

For V1 only the regions closest to the critical point gave matching δ values. The error bars on the δ values in Table II reflect the changes in $\delta_{\pm}$ when different fit regions are examined. In V2 there are regions on both sides of the critical point which yield a matching set of $\delta_{\pm}$ values. No such region could be found for V3, even very close to the critical point. The van der Waals fluid shows some regions on both sides of the critical point where $\delta_{\pm}$ match, to within error bars, and agree with the expected value of $\delta = 3$.

Finally, the topological exponent τ from Fisher's droplet model [35] can be recovered based on considerations of the compressibility factor C_f via the relationship [36]

$$C_f = \frac{\zeta(\tau)}{\zeta(\tau - 1)}. \tag{31}$$

The Riemann ζ functions of Eq. (31) were summed from 1 to 1 000 000 000. When a value of $\tau = 7/3$ was input for the van der Waals fluid, Eq. (31) yielded a value of 0.393 indicating that terminating the summation at 1 000 000 000 yields a value of C_f that is approximately 5% too high; for the van der Waals fluid $C_f = 3/8$. This supposition is supported by decreasing the upper summation limit and observing and increase in the value of C_f. This *error* was accounted for in the estimation of the value of τ. See Table II for results.

TABLE III. Scaling law results.

System	Rushbrooke	Griffiths	Widom	Fisher
V1	2.6 ± 0.4	1.8 ± 0.5	0.9 ± 0.2	-0.5 ± 0.2
V2	3.2 ± 0.5	3.2 ± 0.4	-0.1 ± 0.2	0.5 ± 0.3
V3	3.7 ± 0.3	3.9 ± 0.6	-0.2 ± 0.3	0.4 ± 0.1
vdW	2.0 ± 0.1	2.0 ± 0.4	-0.0 ± 0.2	0.0 ± 0.1

2. Scaling laws

With five critical exponents determined it is possible to perform a consistency check using the well known scaling relations. For example, the Rushbrooke inequality shows that

$$\alpha + 2\beta + \gamma = 2 \tag{32}$$

(here shown as an equality in keeping with the scaling hypothesis and renormalization [37]), and the Griffiths equality

$$\alpha + \beta(1 + \delta) = 2, \tag{33}$$

and the Widom equality

$$\beta(\delta - 1) - \gamma = 0. \tag{34}$$

Finally from Fisher's droplet model

$$\frac{\beta}{\gamma} - \frac{\tau - 2}{3 - \tau} = 0. \tag{35}$$

Using the average values determined for α, β, δ, γ, and τ the results for these scaling laws are compiled in Table III. Only the van der Waals fluid results consistently satisfy the above scaling laws to within error bars. The nuclear models generally fail to satisfy three of the four scaling laws. This failure is inconsistent with the behavior of the phase diagram, shown for example in Fig. 5, which appears show a critical point, thus indicating the presence of a continuous phase transition. While moderately good fits are observed for the specific heat, the *liquid-gas* density difference, the isothermal compressibility and the critical isotherm for each of the versions of the nuclear model, the meaning of these power laws and critical exponents remains an open question in light of the failure to adhere to well-known scaling laws.

V. SUMMARY

It has been shown that the type of nuclear model discussed here exhibits many features commonly associated with a system in which critical phenomena are present, e.g., a coexistence curve, power laws, critical exponents. By removing both the Coulomb and temperature-dependent free energy terms, it was found that the appearance of a critical point in these models is due to the interplay between the surface, volume, and translational free energy terms. However, these types of models are not without inconsistencies. One striking inconsistency is the fact that the temperature-dependent surface free energy gives rise to a infinite negative specific heat at the critical temperature used by the model. Furthermore, no version of the model showed a critical tem-

perature that agreed with the one explicitly input into the surface free energy term. Additionally, when the surface term was rendered temperature independent the critical point remained, thus suggesting that the appearance of a critical point in these models is not dependent on the temperature dependence of the surface term but rather is a result of the interplay between the surface and volume free energy terms.

The critical temperature and density have been determined by examining isotherms in the P-ρ plane. In the neighborhood of this critical point, singular behavior characterized by power laws was observed. However, these critical exponents do not obey well-known scaling relations. This is a particularly troublesome occurrence as any model with true critical behavior, even the simple van der Waals fluid, does have exponents which obey these scaling relations. It is possible that an examination of this model for larger systems, with smaller steps in temperature and volume in the calculation of the free energy, will yield a consistent set of critical exponents.

It is important to note that the critical densities found here are much higher than could be realized with a closest packing of normal density nuclei. Additionally, these critical densities are significantly higher than those typically used to compare model predictions [1,2] to data.

A major conclusion of this work is that the particular phenomenological description of the free energy of a hot nucleus leads to several inconsistencies regarding both temperature and density. It was pointed out that the parameterization of the surface free energy leads to a negative and divergent contribution to the specific heat as T approaches the value of the parameter T_c in Eq. (4). Furthermore, all values of the critical temperature found from examination of isotherms in the P-ρ plane are much below this parameter value. Thus, while use of such a model may well lead to an excellent description of multifragmentation data, the lack of internal consistency noted here makes the interpretation of data in terms of the model problematic. Such agreement may rest more on the phase space sampling and variable free volume inherent in the model than on the finer details examined here. Finally, it has been shown that the variable volume version of this phenomenological model of multifragmentation exhibits caloric curves which can be misinterpreted in the absence of detailed knowledge of the complete thermodynamic phase diagram.

[1] J. P. Bondorf *et al.*, Phys. Rep. **257**, 133 (1995).
[2] D. H. E. Gross, Rep. Prog. Phys. **53**, 605 (1990).
[3] J. Pan and S. Das Gupta, Phys. Rev. C **51**, 1384 (1995).
[4] S. Das Gupta, J. Pan, and M. B. Tsang, Phys. Rev. C **54**, R2820 (1996).
[5] W. Bauer, Phys. Rev. C **38**, 1297 (1988).
[6] S. Pratt, C. Montoya, and F. Ronning, Phys. Lett. B **349**, 261 (1995).
[7] V. Latora, M. Belkacem, and A. Bonasera, Phys. Rev. Lett. **73**, 1765 (1994).
[8] S. Das Gupta and A. Z. Mekjian, Phys. Rev. C **57**, 1361 (1998).
[9] A. S. Botvina *et al.*, Nucl. Phys. **A475**, 663 (1987).
[10] J. E. Finn *et al.*, Phys. Rev. Lett. **49**, 1321 (1982).
[11] R. W. Minich *et al.*, Phys. Lett. **118B**, 458 (1982).
[12] A. S. Hirsch *et al.*, Phys. Rev. C **29**, 508 (1984).
[13] M. L. Gilkes *et al.*, Phys. Rev. Lett. **73**, 1590 (1994).
[14] J. B. Elliott *et al.*, Phys. Lett. B **381**, 35 (1996).
[15] J. A. Hauger *et al.*, Phys. Rev. Lett. **77**, 235 (1996).
[16] J. A. Hauger, P. Warren *et al.*, Phys. Rev. C **57**, 764 (1998).
[17] J. B. Elliott *et al.*, Phys. Lett. B **418**, 24 (1998).
[18] J. Pochodzalla *et al.*, Phys. Rev. Lett. **75**, 1040 (1995).
[19] K. C. Chase and A. Z. Mekjian, Phys. Rev. C **52**, R2339 (1995).
[20] J. Bondorf *et al.*, Nucl. Phys. **A444**, 460 (1985).
[21] J. P. Bondorf, A. S. Botvina, and I. N. Mishustin, Phys. Rev. C **58**, R27 (1998).
[22] M. D'Agostino *et al.*, Nucl. Phys. **A650**, 329 (1999).
[23] C. Kittel, *Thermal Physics* (Wiley, New York, 1979).
[24] D. Stauffer and C. S. Kiang, Adv. Colloid Interface Sci. **7**, 103 (1977).
[25] P. Bhattacharyya, S. Das Gupta, and A. Z. Mekjian, Phys. Rev. C **60**, 064625 (1999).
[26] H. R. Jaqaman, A. Z. Mekjian, and L. Zamik, Phys. Rev. C **29**, 2067 (1984).
[27] J. N. De, B. K. Agrawal, and S. K. Samaddar, Phys. Rev. C **59**, R1 (1999).
[28] D. H. E. Gross, Phys. Rep. **279**, 119 (1997).
[29] E. A. Guggenheim, *Thermodynamics* (North-Holland, Amsterdam, 1993).
[30] N. Goldenfeld, *Lectures of Phase Transitions and the Renormalization Group* (Addison-Wesley, Reading, MA, 1992).
[31] E. A. Guggenheim, J. Chem. Phys. **13**, 253 (1945).
[32] D. J. Wales and R. S. Berry, Phys. Rev. Lett. **73**, 2875 (1994).
[33] D. J. Wales and J. P. K. Doyle, J. Chem. Phys. **103**, 3061 (1995).
[34] P. Heller, Rep. Prog. Phys. **30**, 731 (1967).
[35] M. E. Fisher, Physics (Long Island City, N.Y.) **3**, 255 (1967).
[36] C. S. Kiang, Phys. Rev. Lett. **24**, 47 (1970).
[37] H. E. Stanley, Rev. Mod. Phys. **71**, S358 (1999).